Integration of Self-Assembled Three-Dimensional Photonic Crystals onto Structured Silicon Wafers

Jianhui Ye,[†] Rudolf Zentel,[*,†] Sanna Arpiainen,[‡] Jouni Ahopelto,[‡] Fredrik Jonsson,[§,||] Sergei G. Romanov,[§] and Clivia M. Sotomayor Torres[§]

Department of Chemistry, University of Mainz, Duesbergerweg 10-14, D-55099 Mainz, Germany, VTT Centre for Microelectronics, P.O. Box 1208, FIN-02044 VTT, Finland, and Tyndall National Institute, University College Cork, Lee Maltings, Cork, Ireland

Received March 21, 2006. In Final Form: May 19, 2006

We report on the fabrication of high-quality opaline photonic crystals from large silica spheres (diameter of 890 nm), self-assembled in hydrophilic trenches of silicon wafers by using a novel technique coined a combination of "lifting and stirring". The achievements reported here comprise a spatial selectivity of opal crystallization without special treatment of the wafer surface, a filling of the trenches up to the top, leading to a spatially uniform film thickness, particularly an absence of cracks within the size of the trenches, and finally a good 3D order of the opal lattice even in trenches with a complex confined geometry, verified using optical measurements. The opal lattice was found to match the pattern precisely in width as well as depth, providing an important step toward applications of opals in integrated optics.

Introduction

The strong research effort devoted to photonic crystals (PhCs) is motivated by their potential in designing a novel generation of optoelectronic devices of reduced size, combining aspects of high integration and the ability to control the emission efficiency. In this respect, multifunctional photonic circuits will require architectures in which the positioning, shaping, and coupling of high-quality 2D and 3D PhCs is of critical importance. In contrast to 2D PhCs, which can be fabricated in, for example, silicon-on-insulator platforms by means of well-developed 2D nanolithography,[1] the integration aspect of 3D PhCs poses a great challenge. Assembling 3D PhCs through wafer bonding has been proven to be a complicated and costly procedure,[2] with no straightforward prospect of further integration yet shown. Alternative 3D nanolithography, in which in-situ 3D patterning of polymer templates is followed by their infiltration by high refractive index semiconductors and completed by nanocomposite inversion, seems to be more efficient but still remains a costly process and requires sophisticated equipment. Moreover, 3D lithography methods are not free from limitations. For example, in the holographic technique,[3] the formation of PhC templates in narrow trenches and cavities in substrates is complicated to achieve because of wall shadows and parasitic reflections, whereas the two-photon polymerization is restricted to dimensions of less than 100 μm.[4] Hence, the self-assembly of monodisperse microspheres into opal structures[5−10] remains the favorite route to templates for platform-integrated photonic materials because of its simplicity, flexibility, and low cost. In particular, the preparation of silicon-inverted PhCs on silicon platforms for the telecommunication frequency range is an important target. The accomplishment of this task, however, first of all requires the realization of perfectly crystalline low-refractive-index 3D templates.

Scheme 1[a]

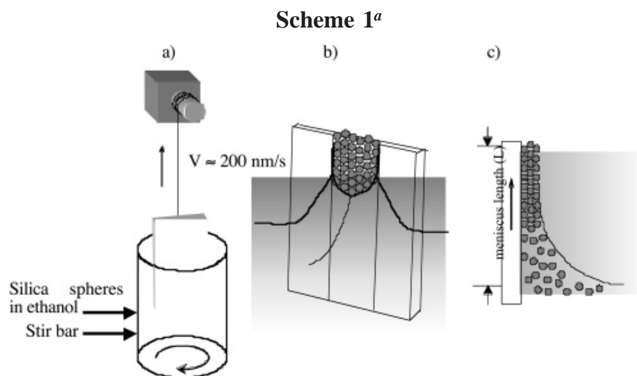

[a] (a) Schematic representation of the crystallization process by drawing up the substrate in a vertical direction with the help of stirring. (b) Crystallization of colloidal crystals on a patterned substrate during withdrawal. (c) Colloid crystallization process in the drying zone.

The quality of self-assembled colloidal crystals on structured silicon wafers depends on the method of fabrication, commensurability of the opal lattice constant, and pattern dimensions, together with a spatial selectivity of opal growth. So far, opals have been crystallized in channel structures, whereby the deposition of opal on top of the wafer surface was mostly prevented by covering it with a slide[6] or by making this surface hydrophobic.[10] These methods are difficult to apply in assembly schemes in micrometer-sized isolated areas. Additional difficulties arise with the crystallization of large spheres because of their lesser Brownian motion and quicker sedimentation, effectively

* To whom correspondence should be addressed. E-mail: zentel@uni-mainz.de.

† University of Mainz.

‡ VTT Centre for Microelectronics.

§ University College Cork.

|| Current address: School of Physics and Astronomy, University of Southampton, England.

(1) Song, B.-S.; Noda, S.; Asano, T.; Akahane, Y. *Nat. Mater.* **2005**, *4*, 207.
(2) Noda, S.; Tomoda, K.; Yamamoto, N.; Chutinan, A. *Science* **2000**, *289*, 604.
(3) Campbell, M.; Sharp, D. N.; Harrison, M. T.; Denning, R. G.; Turberfield, A. J. *Nature* **2000**, *404*, 53.
(4) Serbin, J.; Ovsianikov, A.; Chichkov, B. N. *Opt. Express* **2004**, *12*, 5221.
(5) Yang, P.; Deng, T.; Zhao, D.; Feng, P.; Pine, D.; Chmelka, B. F.; Whitesides, G. M.; Stucky, G. D. *Science* **1998**, *282*, 2244.
(6) Ozin, G. A.; Yang, S. M. *Adv. Funct. Mater.* **2001**, *11*, 95.
(7) Miguez, H.; Yang, S. M.; Ozin, G. A. *Adv. Funct. Mater.* **2002**, *12*, 425.
(8) Yin, Y.; Xia, Y. *Adv. Mater.* **2002**, *14*, 605.
(9) Ferrand, P.; Egen, M.; Griesebock, B.; Ahopelto, J.; Müller, M.; Zentel, R.; Romanov, S. G.; Sotomayor Torres, C. M. *Appl. Phys. Lett.* **2002**, *81*, 2689.
(10) Fustin, C.-A.; Glasser, G.; Spiess, H. W.; Jonas, U. *Adv. Mater.* **2003**, *12*, 1025.

10.1021/la0607611 CCC: $33.50 © 2006 American Chemical Society
Published on Web 07/18/2006

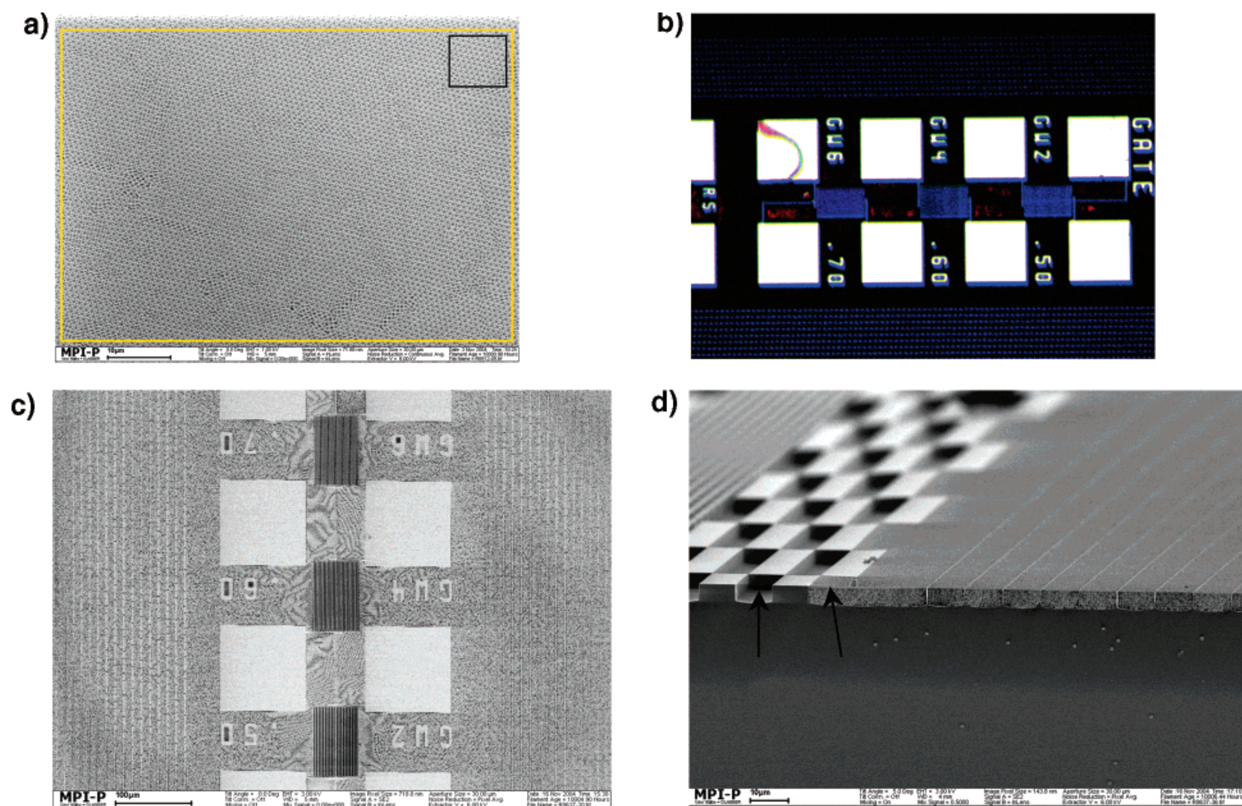

Figure 1. (a) SEM image of crystallized silica spheres on a plain Si substrate. The small black and large white squares represent the areas used for the calculation of the Fourier transforms in Figure 3c and d. (b) Optical micrograph of the etched substrate after the crystallization of silica opals (about 1 mm × 0.7 mm). The high-lying parts of the wafer are uncovered (blank silicon = white); the low-lying etched pattern is completely filled (dark). (c, d) Representative SEM images showing the same selectivity. Notice the difference between isolated trenches and trenches of the same size, which are connected to a continuous trench in part d.

reducing the bead concentration in the meniscus of the air−suspension interface close to the substrate. A combination of directed evaporation-induced self-assembly (DEISA process) and slow stirring to keep the spheres levitated has been suggested as a method for assembling large spheres in channels.[7] However, this method is poor in its control of the opaline thickness, its influence on the selectivity of deposition, and in obtaining large-area opals with high quality. Ozin et al. have reported on the control of the opaline film thickness by heating;[11] however, this method is suitable only for silica spheres with diameters smaller than 500 nm, and the problem of cracks is not solved.

In this article, we for the first time report on the use of a drawing apparatus[12,13] (providing control of the crystallization speed) in combination with stirring (providing counterbalancing of the sedimentation) for the growth of high-quality colloidal crystals from large SiO_2 spheres of 890 nm diameter. This choice of sphere diameter is dictated by the need to match the telecommunication wavelength range and the high-order photonic band gaps of the inverted Si opal targeted by the fabricated SiO_2 templates. Crystallization in a drawing apparatus allows a precise variation of parameters by changing the drawing speed compared to a control of the evaporation rate[11] and can be used to grow high-quality opals. This opens for the possibility of crystallization in selected areas of complex-structured silicon wafers.[9] Hence, we focused on optimizing the opal crystallization conditions in confined geometries of complex topology for the sedimentation of such large SiO_2 spheres. The obtained silica opals are proven to be of excellent quality, which is confirmed by optical as well as scanning electron microscopy studies.

Experimental Section

The patterned silicon substrates were prepared from (100)-polished silicon substrate wafers by etching them in an inductively coupled plasma (ICP) reactor, using the standard Bosch process down to a depth of 5 μm. The substrates were cleaned for 20 min in a 7:3 sulfuric acid (98%)/hydrogen peroxide (35%) solution, followed by hydrophilization in a 1:1:5 H_2O_2 (35%)/NH_3 (28−30%)/H_2O bath at 65 °C for 20 min. The substrates were finally rinsed in deionized water and dried using nitrogen gas. As a result of this process, the whole wafer is highly hydrophilic, the low-lying etched parts as well as unetched high parts. To make silicon 3D photonic crystals, for which the photonic band gap of the replica is in the near-infrared, microspheres made of silica with sizes greater than 850 nm are required. The silica spheres used in the present work were of 890 nm diameter, prepared according to the method of Unger[14,15] and a gift from him. The spheres were cleaned by consecutive centrifugation, decantation, and redispersion in water. Laser diffraction with a "mastersizer"[16] and scanning electron microscopy studies of the silica spheres showed high monodispersity, with a polydispersity index smaller than 2%.

To obtain the colloidal crystals grown in the microscopically structured substrates, the profiled silicon substrates were vertically

(11) Wong, S.; Kitaev, V.; Ozin, G. A. *J. Am. Chem. Soc.* **2003**, *125*, 15589.
(12) Gu, Z. Z.; Fujishima, A.; Sato, O. *Chem. Mater.* **2002,** *14*, 760.
(13) Egen, M.; Voss, R.; Griesebock, B.; Zentel, R.; Romanov, S.; C. M. Sotomayor Torres, C. M. *Chem. Mater.* **2003**, *15*, 3786.
(14) Unger, K.; H. Giesche, H.; Kinkel, J. DE 35 34143A1 Kugelförmige Silica Partikel, Merck Patent GmbH, Sept 25, 1985.
(15) Kaiser, C.; Hanson, M.; Giesche, H.; Kinkel, J.; Unger, K. K. Nonporous Silica Microspheres in the Micron and Submicron Range: Manufacture, Characterization and Application. In *Fine Particle Science and Technology: From Micro to Nanoparticles*; Pelizetti, E., Ed.; NATO AST Series; Kluwer Academic Publishers: Dordrecht, The Netherlands, 1996; pp 71−84.
(16) Mastersizer measurements were made from company Celanese emulsion GmbH by using the Malvern mastersizer microplus instrument. Reference to this method: Kippax, P. *Pharma. Technol. Eur.* **2005** *17*, 32.

lifted out of a colloidal suspension at a controlled slow speed on the order of some 100 nm/s (Scheme 1a). Highly monodisperse colloids together with a rather slow evaporation at the contact line are prerequisites to obtaining highly ordered colloidal layers. As described by Jonas et al.,[17] the shape of the meniscus drives the crystallization. However, in our case we do not rely on a lateral hydrophilic−hydrophobic pattern to change the length of the meniscus. Instead, the capillary forces create a nonuniform meniscus pattern (Scheme 1b), which drives the crystallization to the etched trenches, where most of the solvent evaporates. Because of stronger capillary forces at the low-lying etched trenches (diameter 1−100 μm), the meniscus in these regions extends higher than at the surface. The exact length of the meniscus differs between different trenches, depending on their width and depth. For a trench of 100 μm diameter, it would, however, be several mm long. In connected trenches, the length depends thus on the length of the connected structure and on how (vertically or horizontally) the trench has been drawn out of the suspension. The fact that crystallization happens preferably in the etched trenches opens the possibility to depositing the spheres selectively there, if the thickness of the opaline film can be controlled well. (In other words, if we draw too slowly, the film gets thicker, and the trenches get overfilled. If we draw too quickly, the film gets thinner, and the trenches are no longer filled completely.) The main advantage of this deposition method using a "lifting machine", as compared to concepts that rely on evaporation, is the possibility to control the film thickness, not only by changing the suspension concentration but also by adjusting the drawing speed.

The main problem with large SiO_2 spheres is their rapid sedimentation in their suspension due to their comparatively high mass. The sedimentation is so strong that after a few minutes a thin, clear layer (nearly silica-sphere-free) can be observed at the surface of the suspension. To prevent sedimentation, we added a spinning magnetic bar to the bottom of a homemade glass container of 4 cm diameter and 11 cm height, as illustrated in Scheme 1a, with slow stirring at 100 rpm. In this setup, the surface of the suspension has to be far enough away from the spinning bar so as to ensure that the suspension in the region of the meniscus contacting the patterned substrate is maintained in a quiet state. Nevertheless, tiny oscillations of the sample occur. They may act like oscillations caused by a loud speaker, create mobility in the assembling spheres, and allow better packing.

In a typical run, a substrate is lifted at room temperature (20−26 °C) at a speed of 200 nm/s out of an 8 wt % suspension. Under these conditions, the substrate is lifted by about 18 mm in 24 h while at the same time the meniscus in the container is lowered by about 2 mm because of the evaporation of ethanol. Thus, the evaporation as such has only a minor influence on the speed of the moving meniscus used for crystallization. This makes the method less sensitive to evaporation and humidity than methods that rely on evaporation to move the meniscus.[7,11]

Scanning electron microscopy (SEM) images were taken with a Zeiss Gemini 1530 at acceleration voltages of 0.5−1 kV. Optical properties of the silica opals were evaluated by measuring their reflectance spectra using a Perkin-Elmer Lambda 19 UV/VIS/NIR spectrometer.

Results and Discussion

The first experiments with the drawing apparatus were performed on flat substrates. Figure 1a shows an SEM image of the resulting silica opal. As shown in the Figure, a large, well-ordered, nearly crack-free opal film was obtained. Optical measurements proving the high quality are presented in Figures 4 and 5 and will be discussed later. After optimization, the crystallization was done on patterned substrates. (See Figure 1b and c for a large-scale view of the substrate.) The samples were prepared from a 2−5 vol % (about 8 wt. %) suspension of 890-nm-diameter silica spheres at a drawing speed of 200 nm/s.

(17) Fustin, C.-A.; Glasser, G.; Spiess, H. W.; Jonas, U. *Langmuir* **2004**, *20*, 9114.

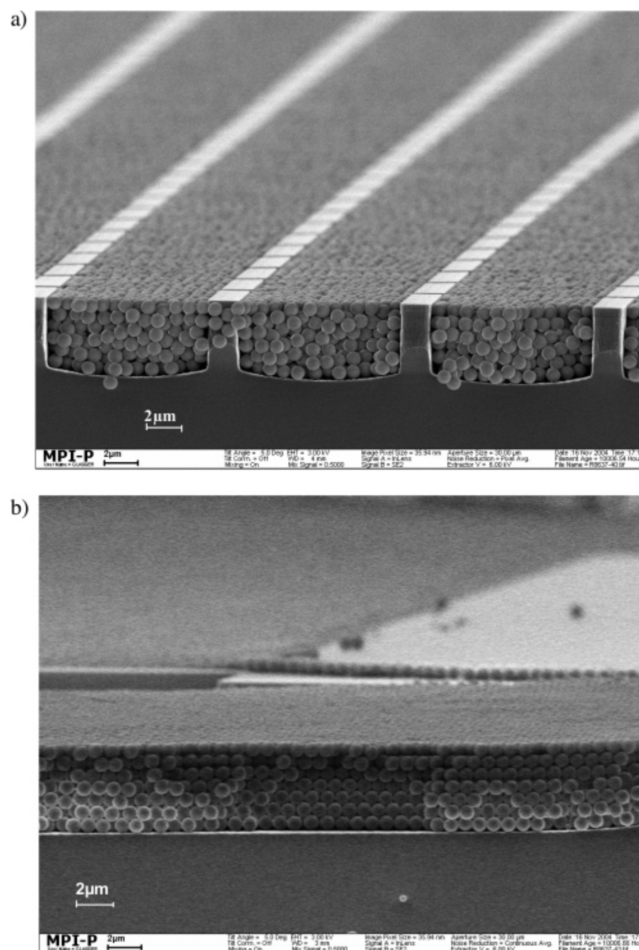

Figure 2. Representative SEM image of the cross section of silica opal on the patterned Si substrate.

Under these conditions, we found it possible to deposit the silica spheres rather selectively onto the profiled substrate, with typical samples shown in Figures 1−3. It should here be pointed out that the samples were neither postprocessed nor cleaned after deposition. The pictures presented show the result immediately after crystallization.

Figure 1b shows an optical micrograph after the self-assembly of the opal. The Figure clearly demonstrates that large-scale silica spheres crystallize exclusively into the etched low-lying trenches and that the unetched (high) parts remain uncovered. The excellent selectivity of the particle deposition can also clearly be seen in the SEM images shown in Figures 1c and d and 2. In Figure 3, very good selectivity is also shown in areas with complex geometry. Even around complex patterns, the filling is highly selective, and the order is very good. Independent of the substrate structure, the deposited film possesses a highly ordered arrangement of silica spheres corresponding to the (111) plane of a face-centered-cubic (FCC) lattice. Noteworthy is the absence of cracking even on large scales, as clearly illustrated in Figure 1a and c. We also studied the silica opals in the third dimension (depth) by SEM imaging of cleaved substrates. Representative SEM images of silica opals at the edges of the cut substrates are shown in Figure 2. These pictures nicely demonstrate that the top surface of the opal is very flat and the order is quite good, in depth as well as in the plane. In particular, this is evident in Figure 2b. In Figure 2a, the order at the edge of a rather narrow trench is destroyed, presumably by the cutting process. In this particular case, the crystal quality may be affected in such narrow trenches either by the slightly concave bottom

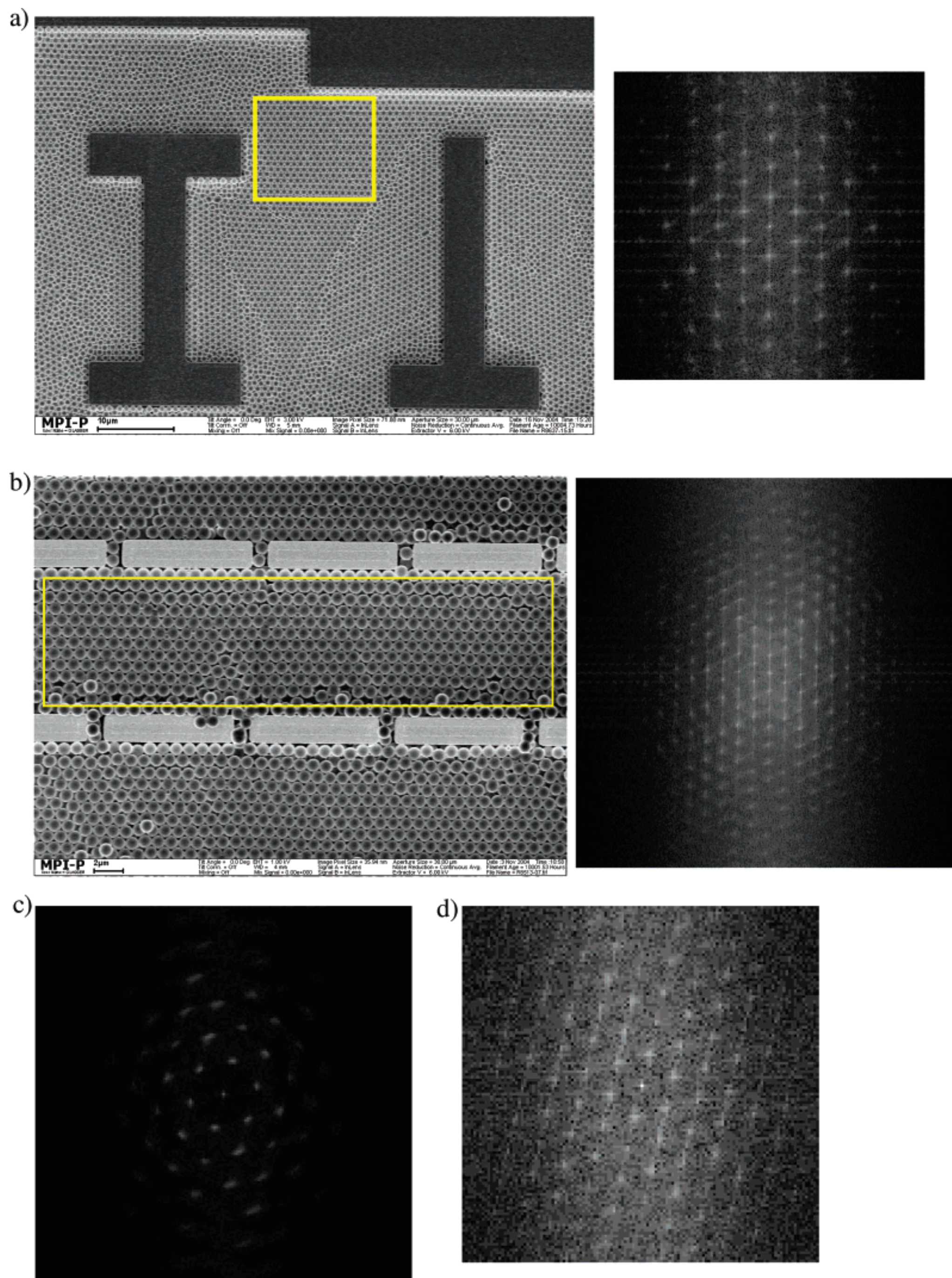

Figure 3. (a) Left: representative SEM image of silica opal on a patterned Si substrate with complex geometry. Right: Fourier transform of a marked region (about 17 spheres × 17 spheres) in an SEM image. (b) Left: SEM image of the same silica opal on another area of the patterned Si substrate. Right: Fourier transform of a marked region (about 38 × 10 spheres) in an SEM image. (c, d) Fourier transform of Figure 1a. (c) Large marked region (about 70 μm × 50 μm). (d) Small marked region (about 10 spheres × 10 spheres).

profile of the etched trenches or by the potential misfit of the lattice dimension to the size of the trench. It is in addition noteworthy that the low-lying trenches are filled up to the top. For the samples presented here, the dimensions of lattice planes and the depths of the trench do match. In cases where they do not match, as in experiments with other wafers or different spheres, the highest layer of spheres is slightly above or below the wafer surface.

The selective deposition scheme as here reported has been realized for samples of 1 cm width and 2 cm height. On inspection of different samples and different regions, it was found that trenches as wide as 110 μm are still completely filled, while the high parts stay sphere-free. The lower limit for structures to be infilled is reached only if their diameter can accommodate only about two spheres. However, with regard to the whole profiled wafer it can be seen that isolated trenches of less than 100 μm length are not entirely filled (Figure 1d), whereas trenches of the same length that are connected to longer trenches are completely filled. In addition, selective filling is possible only if the trenches are oriented perpendicular to the meniscus. This result can be explained only by the fact that the driving force for selective crystallization is the larger meniscus length in the low-lying trenches due to capillary forces, as compared to that in the higher-lying areas. For this to happen, the meniscus must extend far above the liquid surface. Therefore, a low-lying trench cannot be filled immediately as it is lifted over the liquid surface.

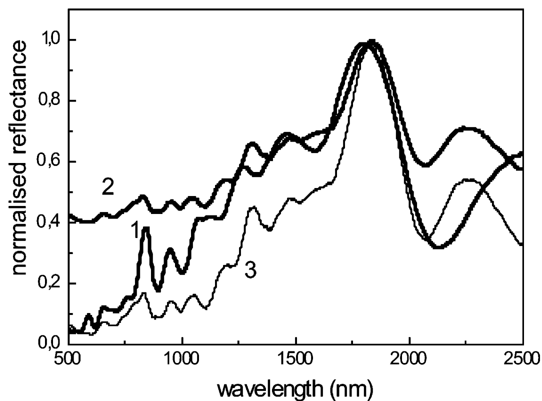

Figure 4. Normalized reflectance spectra of opal on flat (curve 1) and patterned (2) substrates. Spectrum 3 is obtained by subtracting the reflectance of the uncovered Si wafer from spectrum 2.

Crystallization starts only when a trench has reached a certain height above the surface of the liquid, enabling a sufficient meniscus length. For short, isolated trenches, this height obviously exceeds the trench length. This finding offers the selectivity of trench infiltration (Figure 1d): trenches with the same cross section can be either infilled or left empty depending on their length or their connection to a longer trench.

The crystalline quality of the opal assembled on the patterned substrate can be examined in the lateral dimension by applying the spatial Fourier transform to selected areas of the lattice images, as shown in Figure 3, and in the depth of the crystal by optical measurements, as shown in Figures 4 and 5. The Fourier transform in Figure 3 nicely shows the hexagonal order of the (111) opaline crystal plane. The sharpness of the pattern is mostly limited by the lateral confinement of opal in trenches. For example, in Figure 3b the peaks in the Fourier transform are much sharper in the horizontal than in the vertical direction because only a few lattice periods are available in the vertical direction before the end of the channel. Parts c and d of Figure 3 show the corresponding size dependence of the pattern. For a sampling area of only 10 spheres, as corresponding to Figure 3a and b, the sharpness is comparable. The sharpness obtained for a large area shows well-defined peaks in the spatial Fourier transform and hence proves the crystal quality.

To determine the periodicity of the opal lattice in the depth of the trench, optical measurements were performed to compare extended opal crystals on flat substrates with the finite-size crystals confined in trenches in the profiled substrate. The reflectance spectra were collected using a beam with a macroscopic spot size of 9×1 mm^2. In the case of profiled substrates, the spectrum is thus averaged over many trenches or realizations of the opal

Figure 5. (a) Reflectance spectra of an opal film on the flat Si substrate at different angles of light incidence indicated by the numbers on the curves. (b) Reflectance spectra of an opal film on the patterned Si substrate at different angles of light incidence indicated by the numbers on the curves. The reflectance magnitude is corrected for the reflectance of the uncovered Si substrate. (c) Bragg peak angle dispersion for the unstructured wafer. Results from the Bragg equation nonlinear fit: $n_{\mathrm{eff}} = 1.3037$; $d = 705$ nm; particle diameter $D = 865$ nm. (d) Bragg peak angle dispersion for the patterned wafer. Results from the Bragg equation nonlinear fit: $n_{\mathrm{eff}} = 1.3099$; $d = 709$ nm; particle diameter $D = 869$ nm.

lattice, with different lateral extensions. Normalized spectra of opal films on flat and patterned substrates directly show the similarity with regard to the Bragg peak centered at 1830 nm and the spectrum shape, as shown in Figure 4. For a more refined comparison, it is important to consider that an intense background due to the mirrorlike reflectance at the uncovered parts of the silicon substrate is superimposed onto the spectrum of the opal on profiled substrates. This contribution sums up to 40% of the total reflectance intensity. To obtain an absolute magnitude of reflectance, this background was subtracted to fit the 5% background reflectance, characteristic of the opal film on a flat substrate at wavelengths far away from the diffraction resonance. The corrected spectrum for the opal on the patterned substrate (shown as curve 3 in Figure 4) and the extended opal crystal on the flat substrate (curve 1) are rather similar. The relative bandwidth of the diffraction resonance, defined as the ratio of the full bandwidth at half-height of the reflectance band to the band central wavelength, is 0.17 for the films on flat substrates and 0.13 for the films on profiled substrates. These values significantly exceed the theoretically calculated value of 0.056 for the relative bandwidth along the (111) axis of a perfect infinite opal. The major reason for this band-gap broadening is, in our case, the small film thickness,[18] which is prominent in the SEM pictures of cut samples and in the optical evaluation of the Fabry−Pérot oscillations. A film thickness of about six layers of spheres was found for opal films on the patterned substrates (Figure 2), and a film thickness of four layers was found for films on a flat substrate. In addition, inhomogeneous broadening of the diffraction resonance of films on patterned substrates increases as a result of averaging over many lattice realizations in different trenches. Microoptical studies of similar but thicker films in individual trenches on silicon substrate produced the narrower relative bandwidth of 0.08.[19] Taking into account the stronger resonance broadening for thinner films, the opals on patterned and flat substrates possess nearly the same quality.

Measurements of the angular dependence of reflection were performed to obtain more information on the crystal quality. Parts a and b of Figure 5 show angularly dependent reflectance spectra of silica opals on flat and patterned substrates, respectively. The central wavelength of the Bragg diffraction band λ_B follows the Bragg−Snell law well (Figure 5c and d)

$$\lambda_B = 2d({n_{eff}}^2 - \sin \Theta^2)^{0.5}$$

where λ_B is the peak wavelength, $d = (2/3)^{1/2}D$ is the lattice constant along the (111) axis involving the sphere diameter D of the close-packed FCC lattice, Θ is the angle between the incident beam and the normal to the (111) plane, and n_{eff} is the effective refractive index determined by ${n_{eff}}^2 = {n_{sio2}}^2\Phi + {n_{air}}^2(1 - \Phi)$, with Φ being the volume fraction of silica spheres. The best fit to the Bragg−Snell equation (Figure 5c) gives $d =$ 706 nm and $n_{eff} = 1.3037$ for silica opal on flat substrates and $d = 709$ nm and $n_{eff} = 1.3099$ for opals on patterned substrates. Both d values are identical within experimental accuracy. The interplane distance obtained from the Bragg fit agrees well with the 890 nm value estimated from Mastersizer and SEM measurements. The n_{eff} value of 1.304 is in the range expected for a close-packed FCC lattice, with 74 vol % filling of SiO_2 spheres if a refractive index of silica (n_{silica}) of 1.42 is assumed.[20]

In addition to the Bragg reflection, Fabry−Pérot oscillations due to the finite film thickness were observed for opals assembled on both flat and patterned substrates. The observation of well-defined fringes by reflectance spectroscopy indicates[21] that the film thickness does not deviate by more than 10% from the average value over the beam spot area of 9×1 mm^2.

Conclusions

We have developed a route to the crystallization of large monodisperse SiO_2 spheres selectively in hydrophilic trenches in etched silicon wafers with complex geometry. This was achieved with a drawing apparatus that allows for easy control of the crystallization speed.

We achieved a high spatial selectivity of opal crystallization without special treatment of the wafer surface, a precise matching of the opal lattice to the pattern dimensions in width as well as in the depth, a high uniformity of the opal film thickness, and a high, 3D order of the opal lattice. The most prominent quality feature in the presented samples is the very low presence of cracks.

It is worth mentioning that the choice of film thickness was made by bearing in mind further infiltration of these opal films with high refractive index material. Thus, the seemingly insufficient diffraction efficiency of this silica template can be converted to strong omnidirectional photonic band gap attenuation after completing the opal inversion.

Acknowledgment. This work was supported by the European Community under the EU IST-510162 project PHAT and by the Innovationsfond of the State Rhineland-Palatinate. We thank Professor Unger (Inorganic Chemistry, University of Mainz) for providing the silica spheres, G. Glasser (MPI for Polymer Research, Mainz) for the SEM imaging, and Dr. J. Wagner (Fraunhofer Institut Golm) for optical measurements.

LA0607611

(18) Bertone, J. F.; Jiang, P.; Hwang, K. S.; Mittleman, D. M.; Colvin, V. L. *Phys. Rev. Lett.* **1999**, *83*, 300.

(19) Míguez, H.; Yang, S. M.; Ozin, G. A. *Langmuir* **2003**, *19*, 3479.

(20) Lin, Y.; Herman, P. R.; Valdivia, C. E.; Li, J.; Kitaev, V.; Ozin, G. A. *Appl. Phys. Lett.* **2005**, *86*, 121106.

(21) Jiang, P.; Bertone, J. F.; Hwang, K. S.; Colvin, V. L. *Chem. Mater.* **1999**, *11*, 2132.